Supporting Information

In Situ Formation of PBAs Nanoparticles Decorated with 3D Carbon Nanosheet Networks for Superior Hybrid Capacitive Deionization Performance

*Shiyong Wang [a]; Gang Wang [a] *; Yuwei Wang [a]; Haoran Song [a]; Sihao Lv [a]; Tianzhu Li [b]; Changping Li [a] **

[a] School of Environment and Civil Engineering, Research Center for Eco-environmental Engineering, Dongguan University of Technology, Dongguan 523106, Guangdong, China

[b] College of Resources and Environment, Northeast Agricultural University, Harbin 150030, Heilongjiang, China

*Corresponding Authors

E-mail: wghy1979@163.com (G Wang)

licpbit@hotmail.com (CP Li)

1. Experimental Section

1.1 Synthesis of 3DC

Using citric acid as carbon source and SiO_2 nanosphere as template were used. The SiO_2 nanospheres and 3DC were prepared by the Stöber sol-gel method and self-assembly method, respectively. Briefly, citric acid (2 g) and SiO_2 (5 g) were dissolved in 80 mL of deionized water by magnetic stirring. The mixture above was fast froze in liquid nitrogen and then freeze-drying. After that, the production was ground into a fine powder and then heated at 800 °C for 2 h under Ar atmosphere. 3DNC was obtained after filtrated with HF, deionized water, and dried at 80 ℃ in vacuum.

2.2 Synthesis of NiHCF@3DC

NiHCF@3DC composites were synthesized by a chemical co-precipitation route. Basically, 0.12 g 3DC was dispersed in 250 mL deionized water and under ultrasonic for 30 min. Then 0.872 g $NiCl_2$ was added into the former solution, and stirring to form a uniform solution. Then a solution containing 50 mL deionized water and 0.495 g $K_3Fe(CN)_6$ was added into above solution under vigorous stirring. The NiHCF@3DC-2 was collected by centrifugation and vacuum filtration, then washed with deionized water and ethanol by three times before dried in vacuum oven at 100 °C. For comparison, NiHCF@3DC-1 and NiHCF@3DC-3 were synthesized under same condition with the mass of 3DC was 0.08 g and 0.16 g, respectively.

1.3 Materials characterization

The morphologies and structures of the samples were characterized through field emission scanning electron microscopy (FE-SEM, FEI Sirion200) and transmission electron microscopy (TEM, JEM-2010F). The crystal structure and phase composition of the composites were investigated using powder X-ray diffraction (XRD, Bruker D8). Nitrogen adsorption–desorption isotherms were collected at 77 K by using an Autosorb 6B instrument to determine the texture properties of the samples. Thermogravimetric analysis (TGA) was performed with TG209 (NETZSCH Co.). XPS measurements were performed with an ESCALAB 250 (Thermo Scientific, USA) by using Al Kα (hν = 1486.6 eV) X-ray radiation. Inductively coupled plasma atomic emission spectroscopy (ICP-MS) was used to analyze the chemical composition of the NiHCF@3DC-2 samples and concentration of Ni and Fe in the tank after the cyclic test of NiHCF@3DC-2//AC.

1.4 Electrochemical Measurements

Cyclic voltammetry (CV), galvanostatic charge-discharge (GCD), and

electrochemical impedance spectroscopy (EIS) were conducted by using a CHI 660E electrochemical workstation in 1 M NaCl solution. A three-electrode system consisting of a platinum foil as the counter electrode, an Ag/AgCl electrode (saturated KCl) as the reference electrode, and the sample was used as the working electrode. To prepare the working electrodes, a homogeneous slurry of sample, polytetrafluoroethene (PTFE), and carbon black with the mass ratio of 8:1:1 in ethanol was pressed by a rolling mill into a film and dried at 80 °C overnight. The obtained electrodes were pushed onto a titanium mesh which used as current collectors. The specific capacitance (C, F g^{-1}) was calculated from the CV curves as **Equation 1**:

$$C = \frac{\int Idt}{2 \times v \times \Delta V \times m} \quad (1)$$

Where C is the specific capacitance (F g^{-1}), I is the response current density(A), v is the potential scanning rate (V s^{-1}), ΔV is the voltage change (V), and m is the active material mass (g).

1.5 HCDI experiments

To prepare the HCDI electrodes, 82.5 wt% active materials (AC, NiHCF, NiHCF@3DC), 10 wt% carbon black, 6 wt% polyvinyl butyral (PVB), and 1.5 wt% polyvinylpyrrolidone (PVP) were mixed together to obtain a homogeneous slurry. Subsequently, the resulting slurry of solids was cast on a graphite paper (5×7 cm^2) and then dried at 80 °C overnight. The mass of AC, NiHCF, NiHCF@3DC are 100, 80 and 80 mg, respectively. The thickness of AC, NiHCF, NiHCF@3DC are 120, 100 and 100 μm, respectively. The HCDI cell consisting of an activated carbon (AC) electrode, a NiHCF@3DC electrodeand a piece of anion exchange membrane (200 μm, Hangzhou Iontech Environmental Technology Co., Ltd. Zhejiang, China) was denoted as NiHCF@3DC//AC, whereas that consisting of an AC electrode, a NiHCF electrode and a piece of anion exchange membrane was denoted as NiHCF//AC. An ~1.5 mm thick silicon gasket and two pieces of ~120 μm thick nonwoven fabric were used as the spacer and separator of the HCDI cells, respectively. Different concentrations of NaCl and voltages were employed to investigate the desalination performance of the HCDI system in various operation conditions. Ion removal step was conducted by applying a voltage (0.4 V to 1.2 V) for a certain time, while the captured ions were released by applying negative voltage (-0.4 V to -1.2 V) for a certain time. A tank (2.5L) of NaCl aqueous solution with different concentrations (100 to 20000 mg L^{-1}, or 1.7 mM to 341.9 mM) was pumped into the CDI setup by a

peristaltic pump at a flow rate of 9 mL min^{-1}, and then flowed into another tank. An electrochemical workstation (CHI 660E) was used to supply the needed voltage. The changes of effluent conductivity and pH were recorded by an ion conductivity meter and pH monitor systems. The NaCl solution concentration was calculated by a calibration curve according to the conductivity profiles. The ion removal capacity (IRC, Γ, mg g^{-1}), charge consumed (Σ, C g^{-1}), charge efficiency (Λ) and energy consumption (E_{con}) were defined as **Equation 2, Equation 3**, **Equation 4** and **Equation 5**, respectively:

$$\Gamma = \frac{\Phi \times \int (C_0 - C_t) dt}{m} \quad (2)$$

$$\Sigma = \frac{\int i dt}{m} \quad (3)$$

$$\Lambda = \frac{\Gamma \times F}{M \times \Sigma} \quad (4)$$

$$E_{con} = \frac{M \times U \int i \, dt}{\Gamma \times m} \quad (5)$$

Where Φ is the flow rate (mL min^{-1}), C_0 and C_t are the influent and the effluent NaCl concentration (mg L^{-1}), respectively; m is the total mass of the two electrodes (g); i is the current during the adsorption process (A); U is the voltage during the adsorption process (V); F is the Faraday constant (96485 C mol^{-1}); and M is the molar mass of NaCl (58.5 g mol^{-1}).

Table S1. Mass fractions of metallic elements in the as-synthesized NiHCF determined by ICP-MS

Element	Mass fraction/ %
Ni	37.4
Fe	22.4
K	1.43

Table S2. Mass fractions of nitrogen and carbon elements in the as-synthesize NiHCF determined by EA

Element	Mass fraction/ %
N	19.88
C	19.26

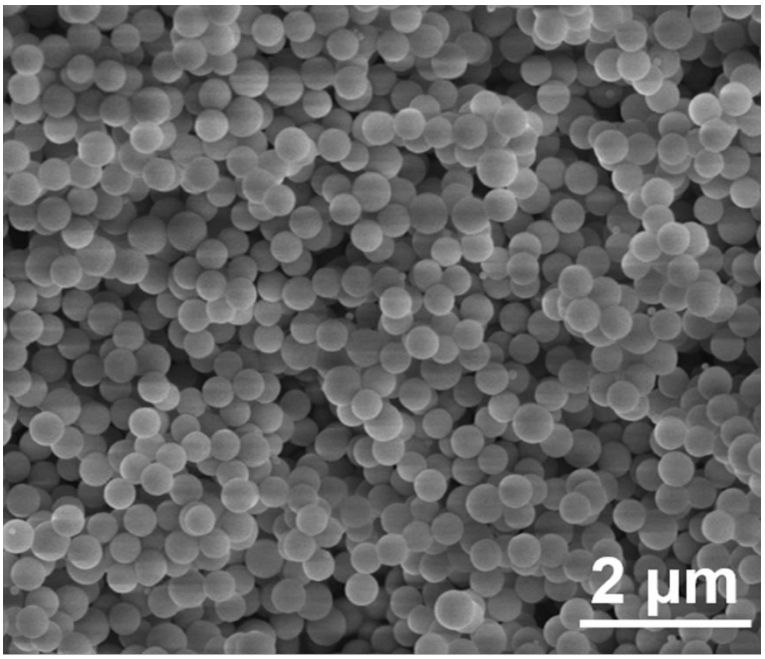

Figure S1. SEM image of SiO_2

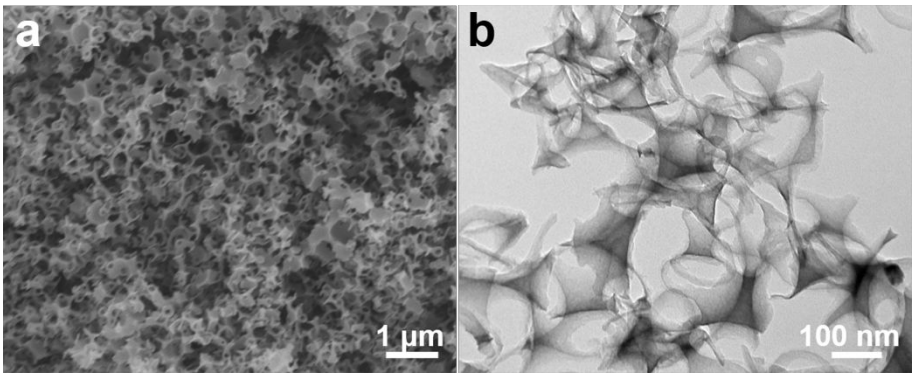

Figure S2. SEM (a) and TEM (b) images of 3DC

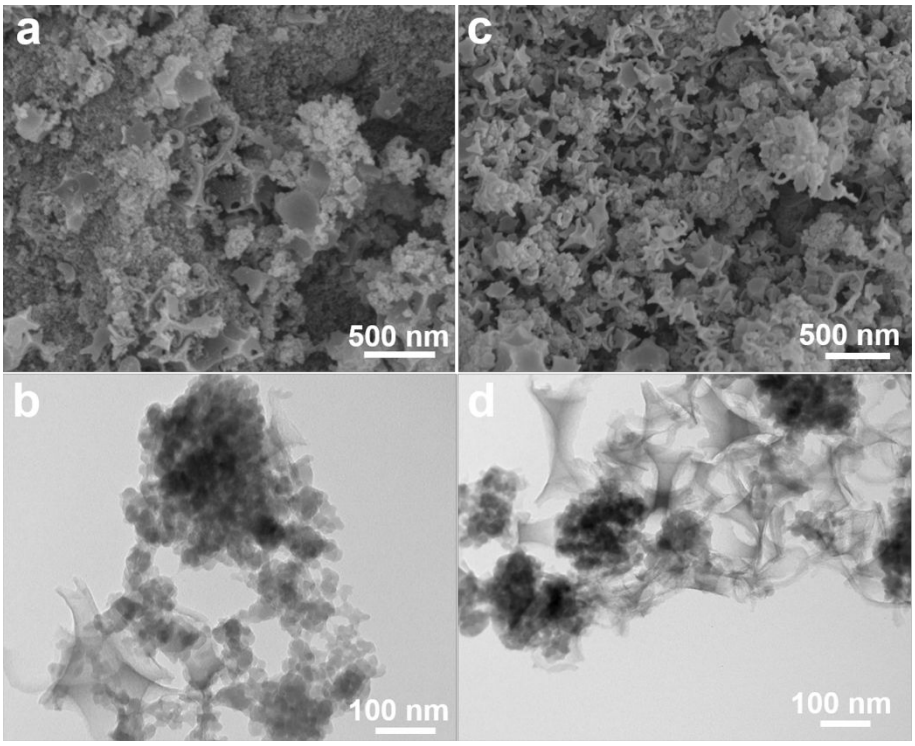

Figure S3. SEM (a) and TEM (b) images of NiHCF@3DC-1; SEM (c) and TEM (d) images of NiHCF@3DC-3

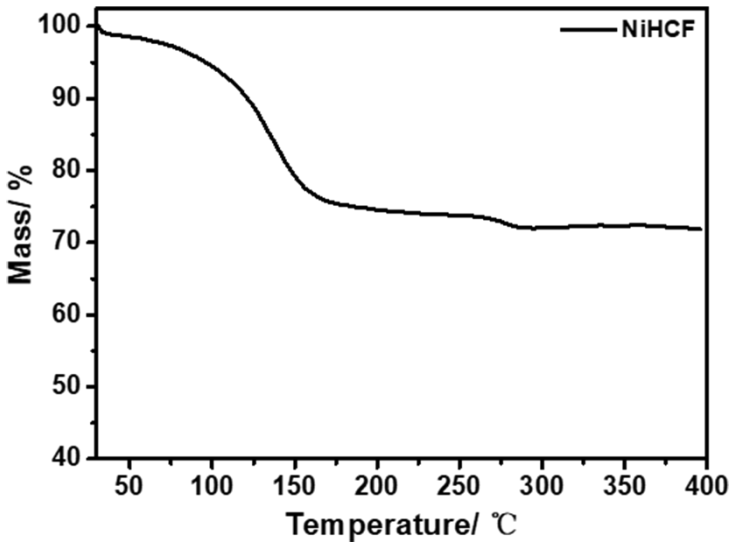

Figure S4. TGA of NiHCF

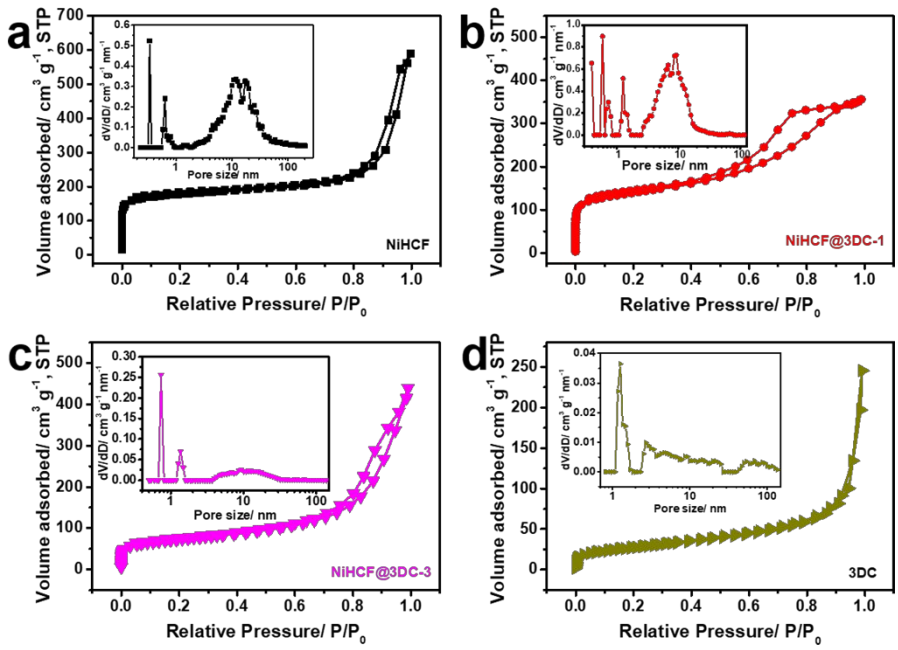

Figure S5. N_2 adsorption/desorption isotherms and pore size distribution (inset) obtained by Barrett-Joyner-Halenda (BJH) of NiHCF (a), NiHCF@3DC-1 (b), NiHCF@3DC-3 (c) and 3DC (d)

Table S3. The D_{Na^+} and BET surface area of samples

Sample	D_{Na^+}/ cm^2 s^{-1}	BET surface area/ m^2 g^{-1}
NiHCF	3.78×10^{-12}	625.1
NiHCF@3DC-1	1.81×10^{-11}	508.4
NiHCF@3DC-2	1.22×10^{-10}	461.2
NiHCF@3DC-3	1.18×10^{-9}	263.1
3DC		98.1

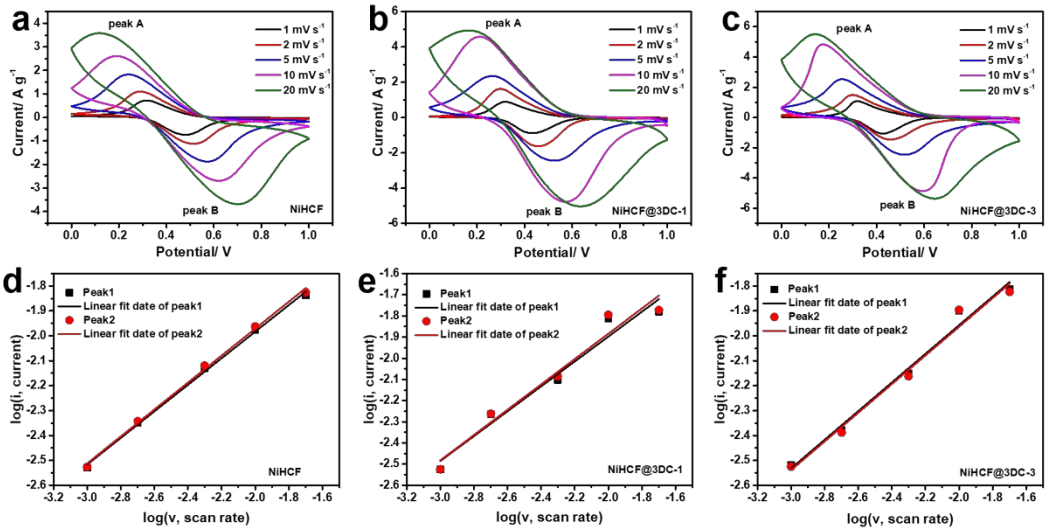

Figure S6. CV curves of NiHCF (a), NiHCF@3DC-1 (b) and NiHCF@3DC-3 (c) at different scan rate; The power-law relation between the peak current and the scan rate of NiHCF (d), NiHCF@3DC-1 (e) and NiHCF@3DC-3 (f)

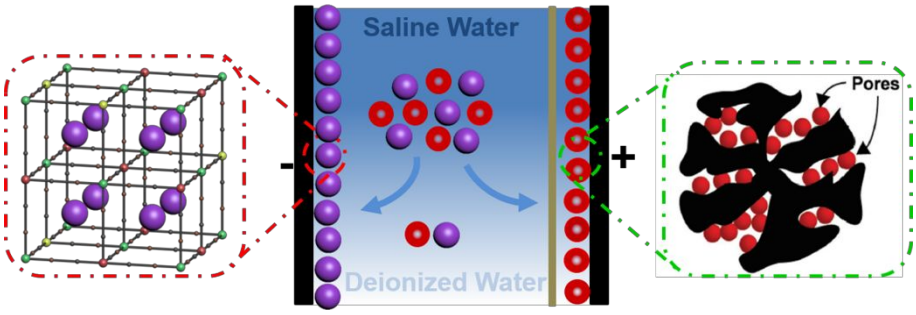

Figure S7. The schematic cell configuration of the HCDI

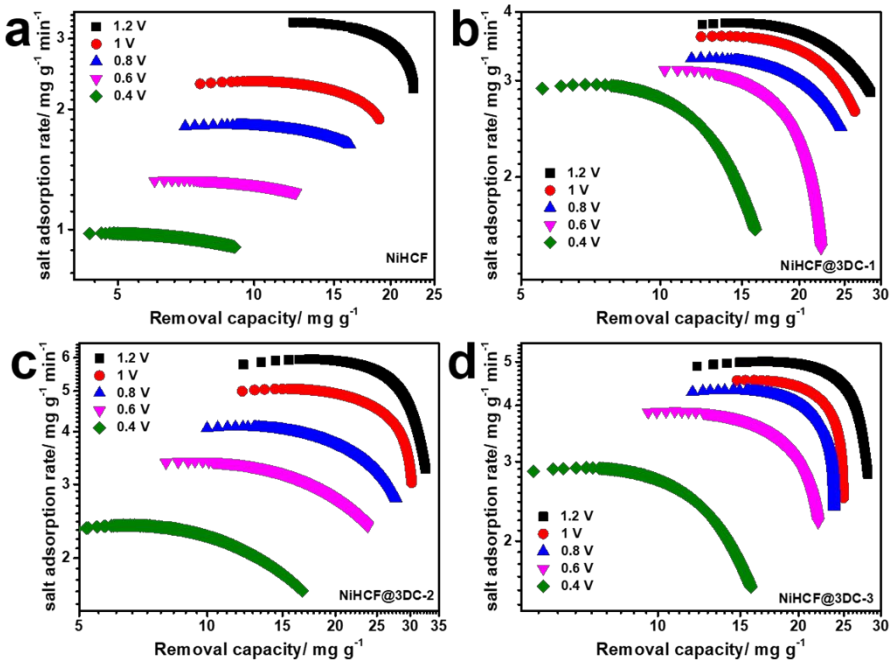

Figure S8. Kim-Yoon plots of (a) NiHCF (a), NiHCF@3DC-1 (b), NiHCF@3DC-2 (c) and NiHCF@3DC-3 (d) in NaCl solution with an initial concentration of 500 mg L^{-1} by varying the cell voltage

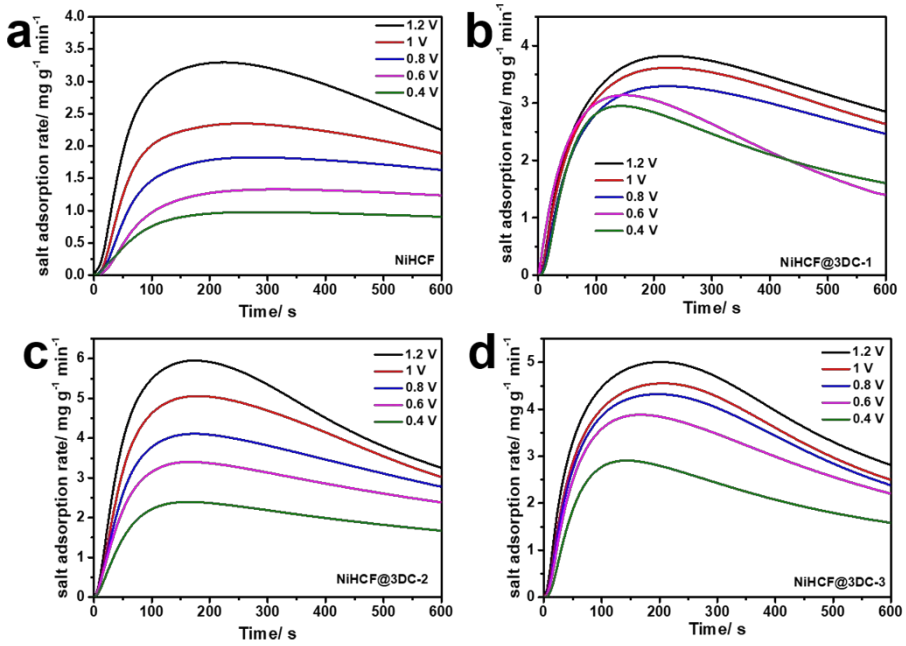

Figure S9. Ion removal rates of (a) NiHCF (a), NiHCF@3DC-1 (b), NiHCF@3DC-2 (c) and NiHCF@3DC-3 (d) in NaCl solution with an initial concentration of 500 mg L^{-1} by varying the cell voltage

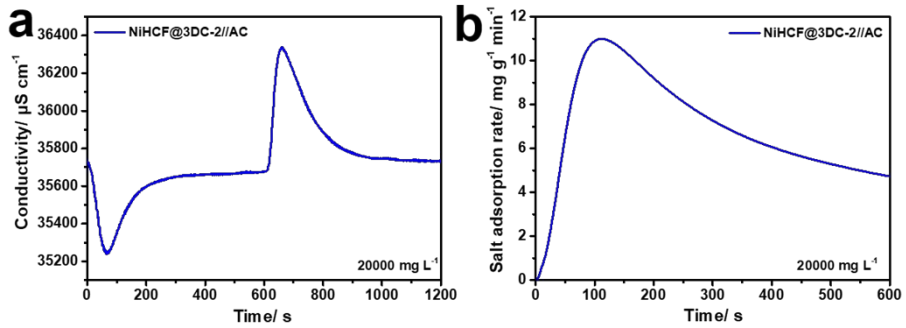

Figure S10 Representative desalination performance (a) and ion removal rates (b) of NiHCF@3DC-2//AC in a 20000 mg L^{-1} NaCl solution at a cell voltage of 1.2 V

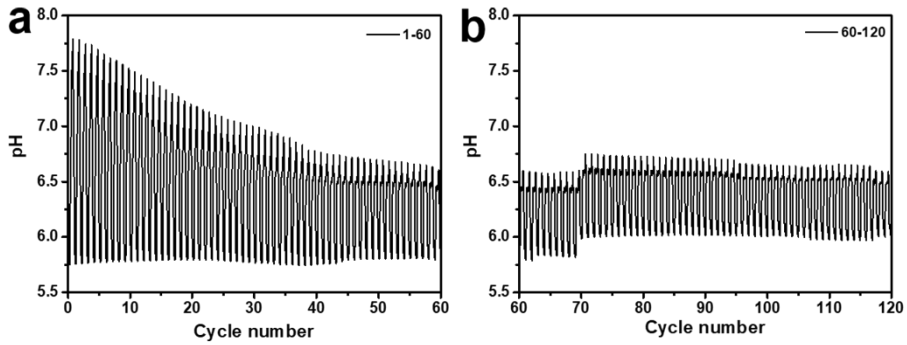

Figure S11. pH changes of the effluent of NiHCF@3DC-2//AC during charge-discharge process in a 500 mg L^{-1} NaCl solution and cell voltage of 0.8 V/-0.8V

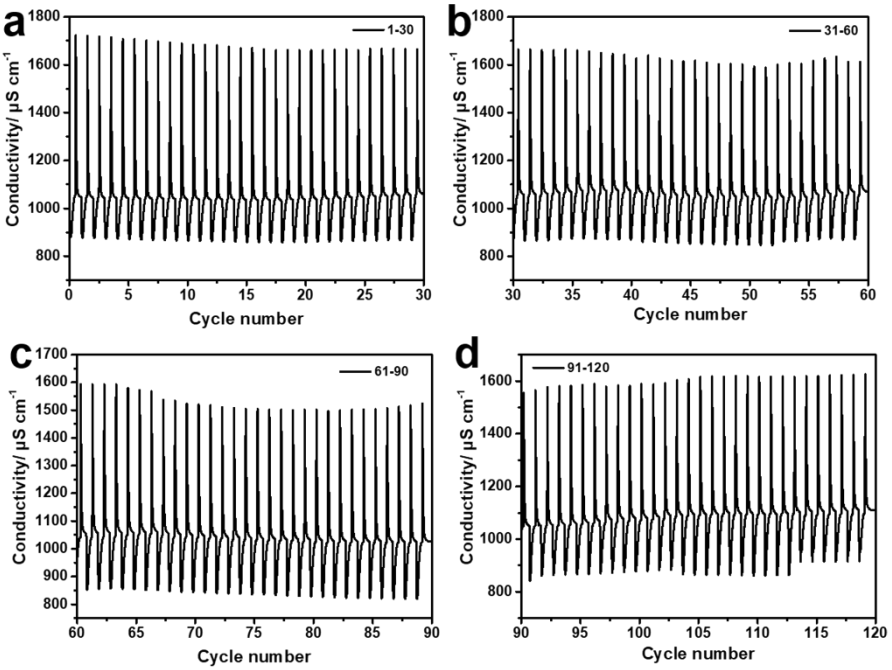

Figure S12. Regeneration stability of NiHCF@3DC-2//AC of 120 adsorption-desorption cycles

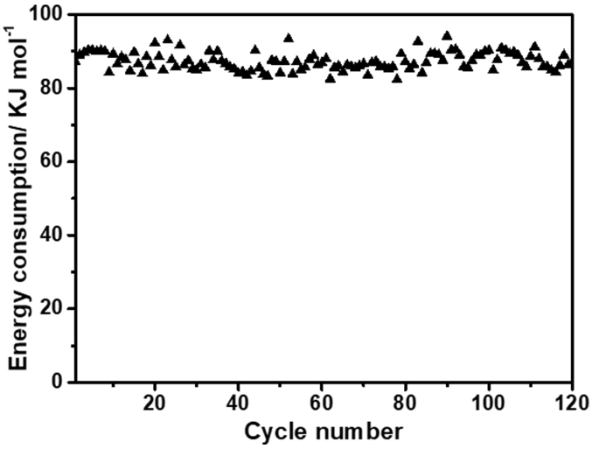

Figure S13 The energy consumption of the NiHCF@3DC-2//AC during cyclic process

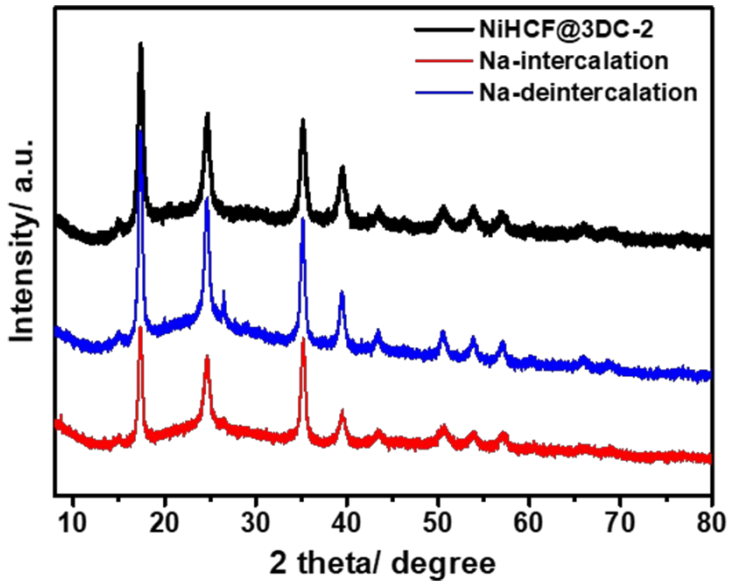

Figure S14. Ex-situ XRD pattern of NiHCF@3DC-2 electrodes before and after the intercalation of cations

Note that the NiHCF@3DC-2//AC was stopped after a couple of cycles when the conductivity curve was stable and then the electrodes were thoroughly washed with deionized water to remove physically ions before analysis.

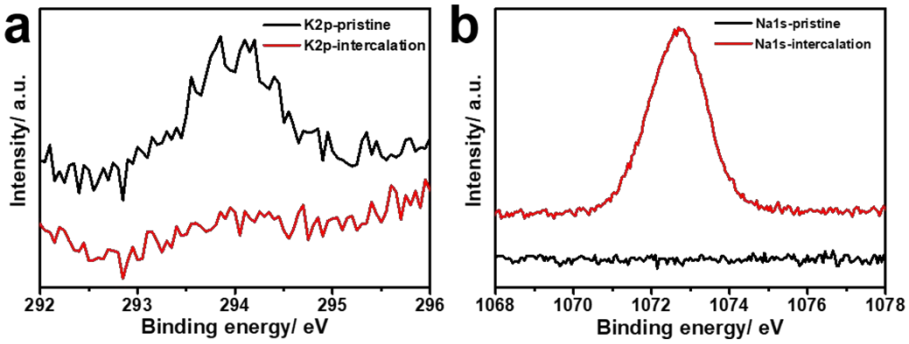

Figure S15. K2p (a) and Na1s (b) XPS of NiHCF@3DC-2 electrodes before and after the intercalation of cations

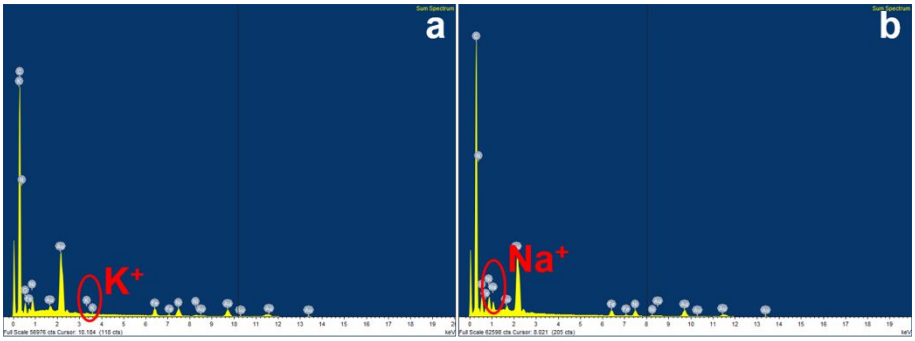

Figure S16. EDS of the NiHCF@3DC-2 electrode before (a) and after (b) the intercalation of cations

Table S4. Comparison of desalination performance among different deionization systems

Materials	Cell configuration	voltage (V)	Current density	Exchange membranes	NaCl (mg L^{-1})	IRC[a] (mg g^{-1})	IRC[b] (mg g^{-1} single electrode)	Ion removal rate (mg g^{-1} min^{-1})
o-OMCs[1]	CDI	1.2	None	None	580	14.58	None	3.1
3D flower-like MoS_2/rGO[2]	CDI	1	None	None	200	16.82	None	None
3DOM-TiN[3]	CDI	1.2	None	None	500	23.6	None	3.2
$K_{0.03}Cu[Fe(CN)_6]_{0.65}\cdot 0.43H_2O$[4]	HCDI	1.2	None	None	4000	23.2	None	14.4
$Na_2FeP_2O_7$[5]	HCDI	1.2	None	Anion	1000	None	30.2	4.86
C@NTO[6]	HCDI	1.4	None	Anion and cation	500	None	49.91	None
α-MnO_2[7]	HCDI	1.2	None	Anion	880	22.1	None	6.66
$Na_4Ti_9O_{20}$[8]	HCDI	1.4	None	Anion	250	None	23.5	None
NaOH-$Ti_3C_2T_x$[9]	HCDI	1.2	None	None	500	16.02	None	None
RGO//Mn_3O_4[10]	HCDI	1.2	None	Anion and cation	1000	None	34.5	1.14
Na-birnessite[11]	HCDI	1.2	None	Anion and cation	880	31.5	None	None
PB/PANI[12]	HCDI	None	100 mA g^{-1}	Anion and cation	500	None	133.3	None
PB/rGA[13]	HCDI	None	100 mA g^{-1}	Anion and cation	2500	130	None	None
CuFe@NiFe PBA[14]	CDI	None	0.5 mA cm^{-1}	Anion	2900	None	71.8	None
NiHCF/rGO-10[15]	HCDI	1.2	None	None	500	22.8	None	None
NTP/C[16]	HCDI	1.6	None	None	1000	None	66.9	None
NiHCF@3DC-2(this work)	HCDI	1.2	None	Anion	500	32.5	73.1	5.1

NiHCF@3DC-2 (this work)	HCDI	1.2	None	Anion	20000	47.8	107.5	11.0

Note:

a. Salt removal capacity based on the total mass of two electrodes

b. Salt removal capacity based on the mass of the single electrode

Reference

(1) Xu, X.; Tan, H.; Wang, Z.; Wang, C.; Pan, L.; Kaneti, Y. V.; Yang, T.; Yamauchi, Y. Extraordinary Capacitive Deionization Performance of Highly-Ordered Mesoporous Carbon Nano-Polyhedra for Brackish Water Desalination. *Environ. Sci.: Nano* **2019,** *6* (3), 981-989.

(2) Peng, W.; Wang, W.; Han, G.; Huang, Y.; Zhang, Y. Fabrication of 3D Flower-like MoS_2/Graphene Composite as High-Performance Electrode for Capacitive Deionization. *Desalination* **2020,** *473*, 114191.

(3) Wu, Y.; Jiang, G.; Liu, G.; Lui, G.; Cano, Z. P.; Li, Q.; Zhang, Z.; Yu, A.; Zhang, Z.; Chen, Z. A 3D Ordered Hierarchically Porous Non-Carbon Electrode for Highly Effective and Efficient Capacitive Deionization. *J. Mater. Chem. A* **2019,** *7* (26), 15633-15639.

(4) Choi, S.; Chang, B.; Kim, S.; Lee, J.; Yoon, J.; Choi, J. W. Battery Electrode Materials with Omnivalent Cation Storage for Fast and Charge-Efficient Ion Removal of Asymmetric Capacitive Deionization. *Adv. Funct. Mater.* **2018**, 28, 1802665.

(5) Kim, S.; Lee, J.; Kim, C.; Yoon, J. $Na_2FeP_2O_7$ as a Novel Material for Hybrid Capacitive Deionization. *Electrochim. Acta* **2016,** *203*, 265-271.

(6) Yue, Z.; Gao, T.; Li, H. Robust Synthesis of Carbon@$Na_4Ti_9O_{20}$ Core-Shell Nanotubes for Hybrid Capacitive Deionization with Enhanced Performance. *Desalination* **2019,** *449*, 69-77.

(7) Byles, B. W.; Cullen, D. A.; More, K. L.; Pomerantseva, E. Tunnel Structured Manganese Oxide Nanowires as Redox Active Electrodes for Hybrid Capacitive Deionization. *Nano Energy* **2018,** *44*, 476-488.

(8) Zhou, F.; Gao, T.; Luo, M.; Li, H. Heterostructured Graphene@$Na_4Ti_9O_{20}$ Nanotubes for Asymmetrical Capacitive Deionization with Ultrahigh Desalination Capacity. *Chem. Eng. J.* **2018,** *343*, 8-15.

(9) Chen, B.; Feng, A.; Deng, R.; Liu, K.; Yu, Y.; Song, L. MXene as a Cation-Selective Cathode Material for Asymmetric Capacitive Deionization. *ACS Appl. Mater. Interfaces* **2020,** *12*, 13750-13758.

(10) Bharath, G.; Naman, A.; Abdul, H.; Fawzi, B.; Dennyson, S.; Hanifa, T.; Mangalaraja, R. V. Synthesis of Hierarchical Mn_3O_4 Nanowires on Reduced

Graphene Oxide Nanoarchitecture as Effective Pseudocapacitive Electrodes for Capacitive Desalination Application. *Electrochim. Acta* **2020**, 337, 135668.
(11) Byles, B. W.; Hayes-Oberst, B.; Pomerantseva, E. Ion Removal Performance, Structural/Compositional Dynamics, and Electrochemical Stability of Layered Manganese Oxide Electrodes in Hybrid Capacitive Deionization. *ACS Appl. Mater. Interfaces* **2018,** *10*, 32313-32322.
(12) Shi, W.; Liu, X.; Deng, T.; Huang, S.; Ding, M.; Miao, X.; Zhu, C.; Zhu, Y.; Liu, W.; Wu, F.; Gao, C.; Yang, S. W.; Yang, H. Y.; Shen, J.; Cao, X. Enabling Superior Sodium Capture for Efficient Water Desalination by a Tubular Polyaniline Decorated with Prussian Blue Nanocrystals. *Adv. Mater.* **2020**, 1907404.
(13) Vafakhah, S.; Guo, L.; Sriramulu, D.; Huang, S.; Saeedikhani, M.; Yang, H. Y. Efficient Sodium-Ion Intercalation into the Freestanding Prussian Blue/Graphene Aerogel Anode in a Hybrid Capacitive Deionization System. *ACS Appl. Mater. Interfaces* **2019,** *11*, 5989-5998.
(14) Zhao, Y.; Liang, B.; Wei, X.; Li, K.; Lv, C.; Zhao, Y. A Core–Shell Heterostructured CuFe@NiFe Prussian Blue Analogue as a Novel Electrode Material for High-Capacity and Stable Capacitive Deionization. *J. Mater. Chem. A* **2019,** *7*, 10464-10474.
(15) Ding, Z.; Xu, X.; Li, Y.; Wang, K.; Lu, T.; Pan, L. Significantly Improved Stability of Hybrid Capacitive Deionization Using Nickel Hexacyanoferrate/Reduced Graphene Oxide Cathode at Low Voltage Operation. *Desalination* **2019,** *468*, 114078.
(16) Wang, K.; Liu, Y.; Ding, Z.; Li, Y.; Lu, T.; Pan, L. Metal–Organic-Frameworks-Derived $NaTi_2(PO_4)_3$/Carbon Composites for Efficient Hybrid Capacitive Deionization. *J. Mater. Chem. A* **2019**, 7, 12126-12133.